A Low-Cost, Intensity-Based Fiber Optic Sensor for Shape-Sensing in Soft Robots

Vedad Bassari

***Abstract*—Fiber optic sensing is a promising approach for shape estimation in soft continuum robots. However, commercial fiber-optic shape sensors are prohibitively expensive for many applications in research and development due to their extensive data acquisition apparatus. Moreover, low-cost solutions that have been developed in research settings lack the sensing range of commercial sensors and can only estimate bending radii for a single curvature. We present a novel fiber optic sensor that enables multi-curve shape sensing with millimeter-scale accuracy via an off-the-shelf camera. This paper introduces a sensor fabrication method based on laser-engraving optical fibers and a data-processing pipeline for interpreting the sensor output. We furthermore provide an analytical model to inform engraving patterns based on the spatial resolution required from the sensor. Finally, we report empirical findings from a soft, multi-curvature joystick that highlights the sensor's unique capabilities.**

***Index Terms*—Modeling, Control, and Learning for Soft Robots, Soft Sensors and Actuators.**

I. Introduction

Continuum 3D shape sensing is challenging due to the richness of the spatial information it requires. However, effective 3D shape sensing is required to take full advantage of the capabilities of soft continuum robots as it enables both environmental mapping via movement and feedback control of the robot's shape. A typical approach to shape sensing is to use resistive or capacitive sensors that change their behaviors under mechanical strain [1]. However, these modes of sensing have little capacity for sensing 3D, multi-curvature shapes due to the limited spatial information they can capture.

One approach to shape sensing is to establish a correlation between the transmission of light through an optical fiber and the curvature of the fiber [2]. Optical signals generated by these sensors can be analyzed for their frequency content or the intensity of the transmitted light. The existing commercial fiber optic shape sensors are limited by the cost and complexity of their signal processing apparatus, which is required by the extensive information they need to process [3]. Several sensors have been developed in a research setting to overcome this limitation and enable curvature measurements for soft muscles [4] and continuum robots [5]. However, these sensors are limited to sensing a single bending radius to circumvent the computational cost of their commercial counterparts.

We propose the use of machine learning and dynamical system modeling tools to address this limitation and develop a low-cost fiber optic sensor built around an off-the-shelf camera sensor that is capable of sensing complex continuum features. To enable the use of these data-processing techniques, we also introduce a repeatable fabrication process to create sensitive, predictable intensity-based fiber optic transducers.

II. Design

A. Hardware Design

The proposed sensor consists of a bundle of 1 mm PMMA optical fibers that are mechanically engraved to become sensitive to bending. By engraving one side of the optical fiber, these sensors leverage the fact that optical rays converge on the convex side of a bent fiber. Thus, bending the fiber in one direction causes the rays to align with the grated zone and refract from the fiber, reducing the intensity of transmitted light. In contrast, bending the fiber in the opposite direction causes the rays to converge on the ungraded zone and reflect into the fiber, increasing the intensity of transmitted light.

This sensing concept has been successfully implemented to sense a single bending radius [6] [7]. However, using the information captured by a bundle of fibers allows shape sensing for multiple bending radii and the detection of intricate deformation patterns. Moreover, individual fibers can be engraved in different spatial patterns to enhance the spatial resolution of the full bundle.

The full sensing system, shown schematically in Figure 1, consists of a fiber bundle that is coupled to an LED on one side, creating a source for optical transmission, and a camera sensor (Thorlabs Inc., Newton, New Jersey, United States) on the other side. The coupling method is intended to precisely constrain the LED, camera, and bundle together to ensure that the optical signals are repeatable and predictable for corresponding mechanical deformations. The information obtained from the camera sensor is then processed through a data-processing pipeline to generate predictions of the bundle's shape.

B. Software Design

The information obtained from the camera sensor is processed by a MATLAB algorithm to make predictions about the bundle shape. The first step in this process is to extract fiber intensities from the camera, which is done by a pixel-based intensity averaging scheme. The user initially selects the location of the fibers in the camera image manually in this scheme.

We will present a simple analytical model for the intensity-bending mapping for this type of sensor in section III. However, it is difficult to create analytical input-output mappings for bundles of fibers with non-linear phenomena that complex engraving patterns can introduce. Additionally, analytical models fail to account for relative movement or twisting of the fibers and similar hardware-associated noise. As a result, we use a feed-forward neural network to create a data-driven, non-linear model of the system's input-output behavior. This

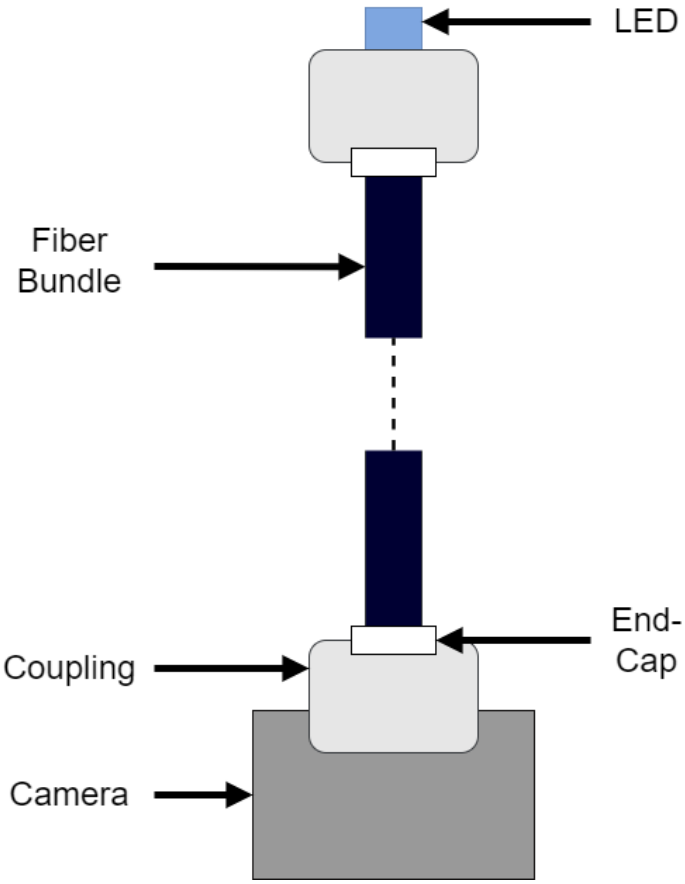

Fig. 1: Schematic of the main components in the system.

neural network is trained on data acquired from an overhead camera that monitors the bundle's 2D shape in a dedicated test fixture. The fiber shape is provided to the network as a set of coordinates, and the network is trained to predict these coordinates based on the intensity vector extracted from the camera. A schematic of this data-processing pipeline is presented in Figure 2. The network used in the subsequent sections consists of two hidden layers with sigmoid activation and is trained using the Levenberg–Marquardt algorithm.

III. Analytical Modeling

The working principle of intensity-based optical fiber curvature sensors was briefly described in section II. More specifically, [8] and [9] show experimentally and computationally that for small radii of bending, the relationship between intensity loss and sensor curvature is approximately linear in sensors with a single engraving. The goal of this section is to extend and validate this model for fibers with multiple engravings which, as discussed before, can enable greater sensing fidelity. While the system presented in this paper relies on a data-driven input-output model, this analytical model serves to both validate the working principle and inform the engraving patterns used in the design of the sensors.

Starting from the single engraving case, a simple linear relationship is given by

$$\begin{aligned} I &= h - C \cdot \theta \qquad (1) \\ C &= C_{convex} \text{ if } \theta \leq 0 \\ C &= C_{convex} \text{ if } \theta > 0 \end{aligned}$$

(2)

where θ is the bending angle at the location of the engraving, I is the normalized intensity, and h is the baseline intensity with no bending. Note that C_{convex} and $C_{concave}$ are linear empirical (rather than model-based) parameters. These parameters are allowed to be different from each other in magnitude in this model - we hypothesize that $|C_{convex}| > |C_{concave}|$ due to the directional sensitivity of the gratings.

A simple extension of this model to the case of a bundle of fibers with two or more engravings per fiber is then given by an equivalent vector equation

$$\begin{aligned} \vec{I} &= \vec{h} - C \sum_{i=1}^{n} \vec{\theta_i} \qquad (3) \\ C &= C_{convex} \text{ if } \theta \leq 0 \\ C &= C_{convex} \text{ if } \theta > 0 \end{aligned}$$

(4)

where n is the number of engravings and θ_i is the local bending angle of the engravings. A key outcome of this model is that a fiber bundle with m engraved fibers can sense up to m local bending radii, which was used as a preliminary benchmark in prototyping. Additionally, greater spatial resolution can be achieved with fewer fibers using multiple engravings per fiber. This premise holds as long as the engravings of the different fibers are not identical and can therefore be used to de-convolve the summation in equation (4). Importantly, however, the number of engravings on a single fiber is limited by the fact that $h < C \sum_{i=1}^{n} \theta_i$ would result in a loss of signal. In practice, $h >> C \sum_{i=1}^{n} \theta_i$ is advisable to increase the signal-to-noise ratio, so at most two engravings were used per fiber in the sensors presented in this paper.

IV. Fabrication

Several prototypes were created with various engraving patterns and different numbers of fibers informed by the model presented in section III. The final prototype bundle was fabricated in a length of approximately 32 cm with 16 fibers that were engraved in a step-wise manner, such that the engravings covered the entire length of the bundle. The fibers were each engraved once with a 2 cm sensitized zone. The engravings were created by a 30-watt laser cutter creating parallel cuts with a 0.025 mm spacing on the fiber at a speed of 1 m/s and a power of 10 W. The cutting parameters were determined empirically by measuring fiber sensitivity for different cutting configurations using a custom test fixture, with the results shown in Figure 3. The settings yielding the largest sensitivity were selected for prototyping.

The fibers are held together by a piece of heat-shrink tubing that is formed around the bundle while the fibers are held in a

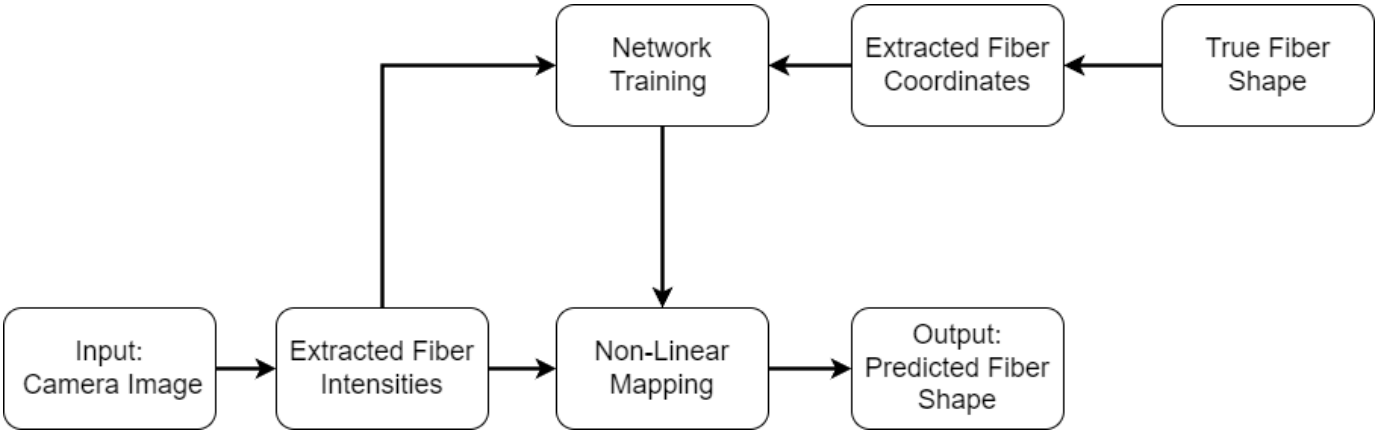

Fig. 2: Schematic of the data-processing pipeline. The true fiber shape is inferred via a secondary overhead camera that monitors the bundle.

fixture. The ends of the fibers are constrained by laser-cut end-caps, epoxied, and sanded down to provide a uniform surface finish at the points of optical coupling. The couplings are accomplished via custom 3D printed components that admit a forced mechanical fit to the end-caps on one end and the LED or camera on the other. The fabricated bundles were then characterized using the data-processing procedure outlined in Figure 2. The training used several hundred samples of input-output data collected from multiple recordings to provide robustness against signal variability.

A. Soft Joystick Demonstration

To demonstrate the unique multi-bend sensing capability of the optical fiber, a soft joystick was designed to enable a user to digitize custom geometric shapes via a computer interface. Such an interface could be used to control the shape of continuum robots among other applications. The joystick was created by casting a hollow cylinder of soft silicone rubber. The fiber bundle was embedded in the cylinder and fixed at the two ends. Custom end fittings were then assembled to couple the joystick to an LED and a portable USB camera which was connected to a real-time implementation of the data-processing algorithm. An image of the demonstration setup is shown in Figure 4.

V. Results

A. Bending Model Validation

The experiments presented in this section aimed to validate the analytical model presented in section III. To begin, an individual fiber with a single engraving was subjected to two experiments that used a photo-resistor to quantify the transmission intensity through the fiber. The first experiment varied the bending angle over the engraved section of the fiber while keeping the insensitive zone straight via fixtures on an optical table. This experiment was then repeated with the insensitive zone bent over various angles while the sensitive zone was held straight. The results, shown in Figure 5(a), confirm the model by showing that the bending only resulted in a variation of transmission intensity when applied to the sensitive zone.

The second set of experiments was performed on a fiber that was engraved in two locations. These experiments changed the bending angle of each sensitive zone separately, as highlighted in Figure 5(b). Note that the bending angle shown in the x-axis of this plot corresponds to that of the first engraving, while each plotted line corresponds to a discrete bending angle of the second engraving. As expected, the transmitted intensity changes linearly with respect to the bending of the first engraved region with two distinct slopes corresponding to the convex and concave bending regimes. A line of best fit is shown for the reference curve $\theta = 0$. Importantly, bending the second engraving adds a secondary shift in transmission intensity which is consistent with the analytical model.

B. Sensor Characterization

The next experiments were performed on the prototype bundle using the same fixture that was used to train the data-processing pipeline. Figure 6 shows the estimated sensor shape as well as the true sensor shape captured by the overhead camera system for various single and multi-curve geometries. Note that both the optical intensity and the fiber coordinates are normalized to simplify the computations. The first plot shows the performance of the network in predicting the bundle shapes from a video that was used in training - although the frames used were divided into separate training and testing batches. The second plot shows the performance of the same network from a different video recording; the prediction accuracy is noticeably worse, though the approximations remain physically grounded. This difference in performance can be quantified by the mean prediction error of the sensor, which rose from 0.00132 ± 0.0001 to 0.0184 ± 0.003 (n = 6) between the two configurations. The latter value corresponds to a mean positional error of 2.21 ± 0.4 mm over the length of the fiber.

C. Soft Joystick Demonstration

Figure 7 shows two shapes that were provided to the user and their corresponding digital twin created through the joystick. The demo highlights the sensor's ability to approximate

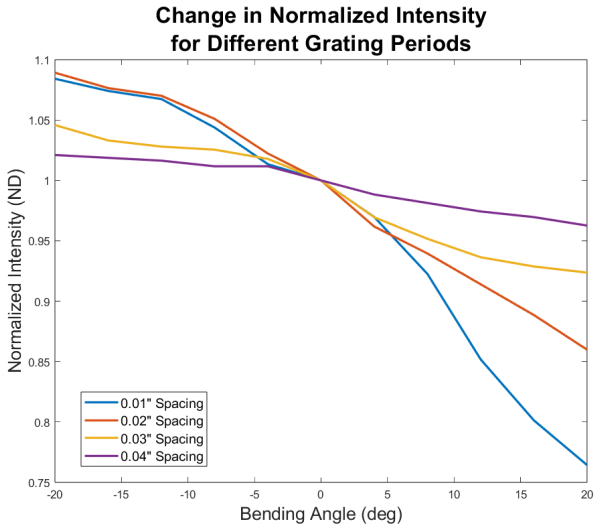

((a)) Fiber transmission intensity for various engraving periods.

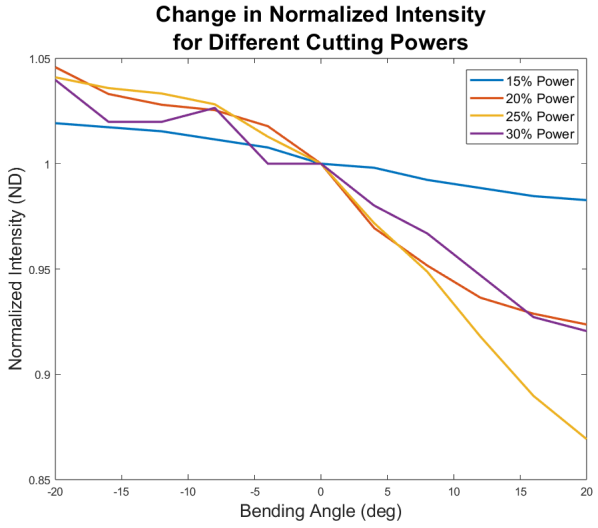

((b)) Fiber transmission intensity for various cutting powers.

Fig. 3: Selected results from laser-engraver parameter selection experiments.

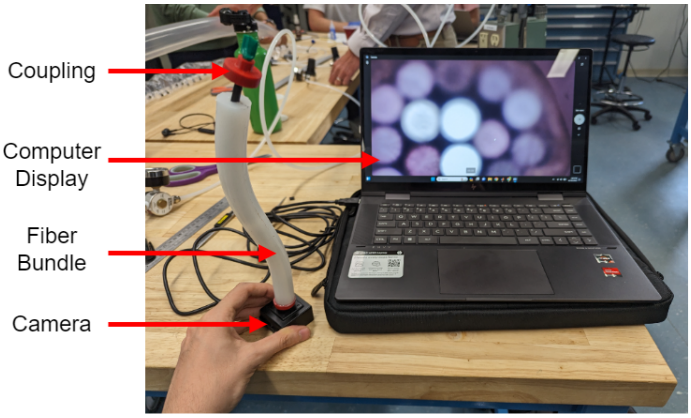

Fig. 4: Annotated picture of the joystick demonstration. The data processing pipeline can be executed on a typical personal computer.

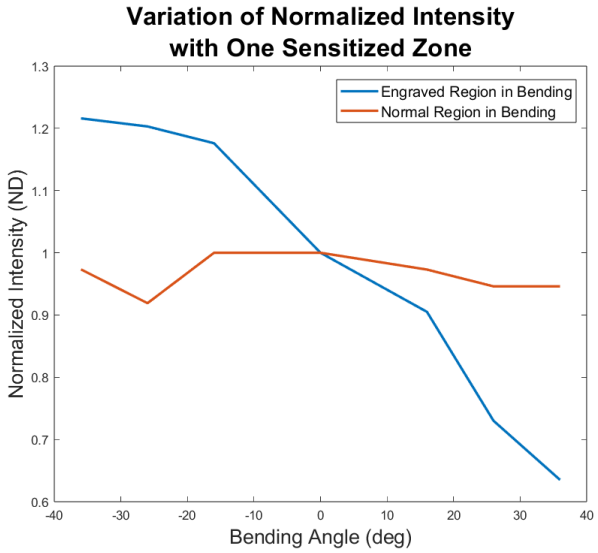

((a)) Fiber transmission intensity for various bending angles of the insensitive and sensitive regions. Bending the insensitive region creates no meaningful signal.

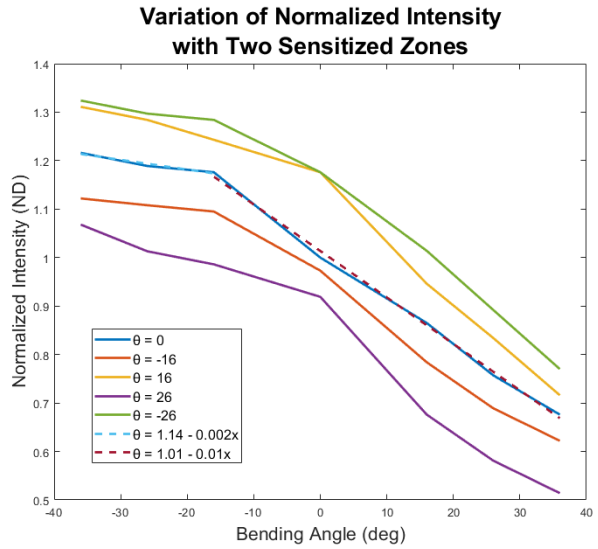

((b)) Fiber transmission intensity for various bending angles of the two sensitive regions. Bending the second sensitive region creates a secondary signal.

Fig. 5: Selected results from model-validation experiments.

the shape of the joystick in real time. However, the resulting signals indicate a reduced accuracy in comparison to the bench-top results presented above despite the sensor being re-trained after implementation in the joystick.

VI. Discussion

The experimental results highlight several features of the sensing system in its current configuration. Importantly, the outcome of Figures 5(a) and 5(b) validates the working principle of the sensor as represented in the analytical model. However, it is noteworthy that the model becomes convoluted for multi-fiber, multi-engraving bundles. Additionally,

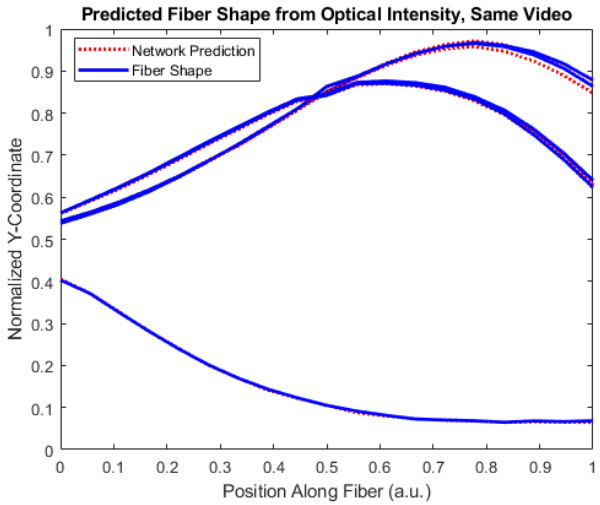

((a)) Training and test data from the same recording.

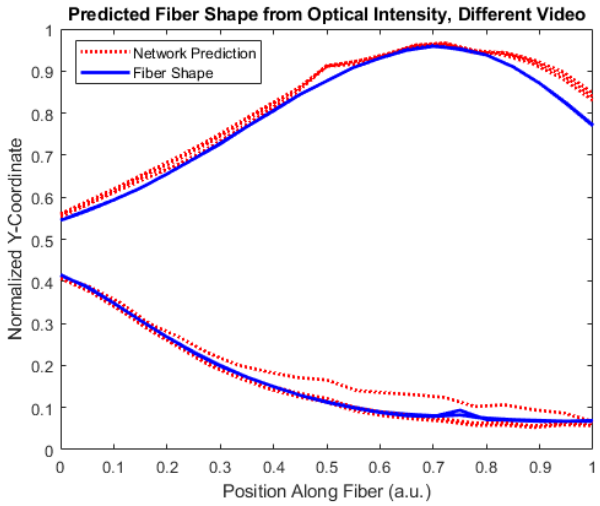

((b)) Training and test data from different recordings.

Fig. 6: True bundle shapes and network-predicted shapes for different geometric configurations of the sensor. The accuracy is reduced when test data is from a different recording than the training data.

the analytical model does not capture various sources of error associated with the physical system, including changes in optical couplings, sliding and relative mechanical movement of the fibers, and torsional motion of the fibers. This additional complexity motivates the use of the adopted data-driven characterization method. Nonetheless, the model is a valuable design tool for sensor fabrication.

Furthermore, the discrepancy seen in Figure 6 highlights the variability of the system's output signal. Several approaches are proposed for handling this limitation: a computational approach is the use of more training samples from different recordings to enhance the computational model's robustness. However, the hardware sources of variability that were discussed above will need to be addressed using more careful fabrication and testing techniques to achieve greater sensing

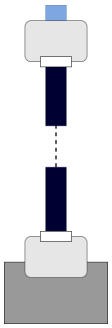

((a)) Shape 1.

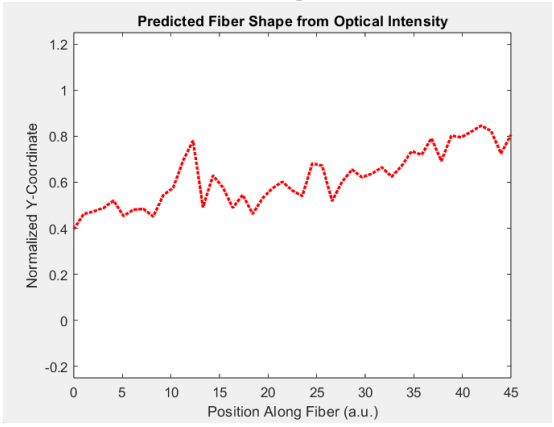

((b)) Digital render of shape 1.

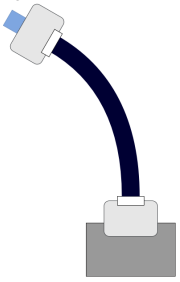

((c)) Shape 2.

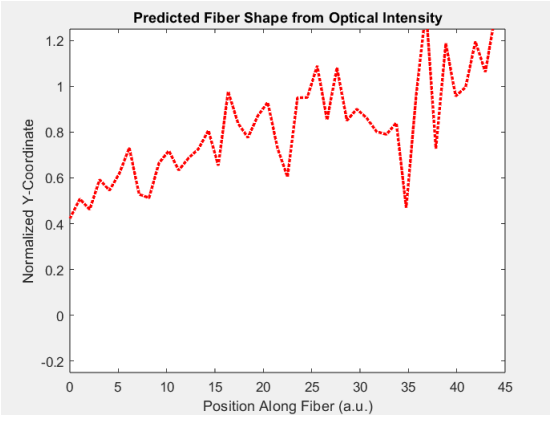

((d)) Digital render of shape 2.

Fig. 7: The shapes shown to the user and the digital shapes created by the user via the sensor. The sensor roughly approximates the physical shapes in real time.

accuracy. These measures will ideally push the positional error of the sensor from 2.21 ± 0.4 mm to the sub-millimeter standards of commercial sensors [10]. Moreover, the testing presented in this paper was confined to planar, quasi-static measurements which are yet to be extended to dynamic scenarios. We note, however, that the positional accuracy of the sensor is comparable to the simpler intensity-based single-curvature sensors [5].

Finally, the challenges affecting the outcome of the soft joystick demonstration highlight the difficulties of embedding the sensor into a portable, real-time form factor. There are several potential causes for the limited accuracy of the sensor in the demonstration. Firstly, to make the joystick portable, the camera sensor was used without a lens - this resulted in lower resolution and a limited field of view and can be addressed with a more careful selection of optical components. Secondly, the training method was intended for 2D shape sensing, so undesirable 3D deformations of the joystick were likely to impact the fidelity of the sensor predictions. Separate 3D training procedures will need to be devised specifically for different implementations of the sensor. Lastly, embedding the bundle in the silicone frame resulted in an additional mechanical constraint which could have further contributed to undesirable twisting and relative motion of the fibers. This highlights the need to model contact mechanics to guide the mechanical integration of the sensor [5].

VII. Conclusion

We presented a novel, low-cost fiber optical intensity-based shape sensor for soft robots along with an analytical model to inform sensor design. The sensor uses off-the-shelf electrical equipment, cheap fabrication methods, and a data-driven characterization method to simplify the data-acquisition complexity associated with fiber optical shape sensors while enabling the measurement of complex geometric shapes not accessible to simpler electro-mechanical sensors. The prototypes shown in the paper provide a proof of concept for the working principle of the sensor. With the foundational concepts demonstrated, the sensor resolution can be improved using a combination of more rigorous software and hardware solutions.

References

[1] O. Medina, A. Shapiro, and N. Shvalb, "Resistor-based shape sensor for a spatial flexible manifold," *IEEE Sensors Journal*, vol. 17, no. 1, pp. 46–50, 2017.

[2] S. C. Ryu and P. E. Dupont, "Fbg-based shape sensing tubes for continuum robots," in *2014 IEEE International Conference on Robotics and Automation (ICRA)*, 2014, pp. 3531–3537.

[3] "Fiber optic sensing and non-destructing testing products — luna," lunainc.com, 2023. [Online]. Available: https://lunainc.com/product-category/sensing-and-non-destructive-test-products#category-13

[4] S. C. Ryu and P. E. Dupont, "Fbg-based shape sensing tubes for continuum robots," in *2014 IEEE International Conference on Robotics and Automation (ICRA)*, 2014, pp. 3531–3537.

[5] W. Chen, C. Xiong, C. Liu, P. Li, and Y. Chen, "Fabrication and dynamic modeling of bidirectional bending soft actuator integrated with optical waveguide curvature sensor," *Soft Robotics*, vol. 6, no. 4, pp. 495–506, 2019, pMID: 30907704. [Online]. Available: https://doi.org/10.1089/soro.2018.0061

[6] A. Djordjevich and M. Boskovic, "Curvature gauge," *Sensors and Actuators A: Physical*, vol. 51, no. 2, pp. 193–198, 1995. [Online]. Available: https://www.sciencedirect.com/science/article/pii/0924424795012222

[7] J. Metz, "Closed loop control of continuum robot using an intensity-based optical fiber bend sensor," in *UC Santa Barbara, ME225EH Soft Robotics*, 2022.

[8] A. Djordjevich, M. Fung, and R. Y. K. Fung, "Principles of deflection-curvature measurement," *Meas. Sci. Technol.*, vol. 12, p. 1983, 2001.

[9] M. Kovacevic, D. Nikezic, and A. Djordjevich, "Monte carlo simulation of curvature gauges by ray tracing," *Measurement Science and Technology*, vol. 15, p. 1756, 07 2004.

[10] K. C. Galloway, Y. Chen, E. Templeton, B. Rife, I. S. Godage, and E. J. Barth, "Fiber optic shape sensing for soft robotics," *Soft Robotics*, vol. 6, no. 5, pp. 671–684, 2019, pMID: 31241408. [Online]. Available: https://doi.org/10.1089/soro.2018.0131